HHS Public Access

Author manuscript

Biomaterials. Author manuscript; available in PMC 2024 September 01.

Published in final edited form as:

Biomaterials. 2023 September ; 300: 122179. doi:10.1016/j.biomaterials.2023.122179.

Self-oxygenation of engineered living tissues orchestrates osteogenic commitment of mesenchymal stem cells

Shabir Hassan[1,4,⊥], **Ting Wang**[1,⊥], **Kun Shi**[1,⊥], **Yike Huang**[1], **Mariely Urbina**[1], **Kaifeng Gan**[1], **Mo Chen**[1], **Niels Willemen**[1,2], **Haroon Kalam**[3], **Eder Luna-Ceron**[1], **Berivan Cecen**[1], **Gihan Daw Elbait**[4], **Jinghang Li**[1], **Luis Enrique Garcia-Rivera**[1], **Melvin Gurian**[2], **Mudassir Meraj Banday**[5], **Kisuk Yang**[6,7], **Myung Chul Lee**[1], **Weida Zhuang**[1], **Castro Johnbosco**[2], **Oju Jeon**[8], **Eben Alsberg**[8,9], **Jeroen Leijten**[2,*], **Su Ryon Shin**[1,*]

[1]Division of Engineering in Medicine, Department of Medicine, Harvard Medical School, and Brigham and Women's Hospital, Cambridge, MA, 02139, USA.

[2]Department of Developmental Bioengineering, Faculty of Science and Technology, TechMed Centre, University Twente, Enschede, 7522 NB, Netherlands.

[3]Infectious Disease and Microbiome Program, Broad Institute of MIT and Harvard, Cambridge, MA, 02139, USA.

[4]Department of Biology, College of Arts and Sciences, Khalifa University, Abu Dhabi P.O. Box 127788, United Arab Emirates.

[5]Department of Medicine, Harvard Medical School, and Brigham and Women's Hospital, Boston, MA, 02115, USA.

[6]Center for Nanomedicine, Department of Anesthesiology, Perioperative and Pain Medicine, Brigham and Women's Hospital, Boston, MA 02115, USA.

[7]Division of Bioengineering, College of Life Sciences and Bioengineering, Incheon National University, Incheon, 22012, Republic of Korea.

[*]Correspondance at: Department of Developmental BioEngineering of the TechMed Centre, University iof Twente, 7522 NB, Enschede, Netherlands. Division of Engineering in Medicine, Department of Medicine, Harvard Medical School, and Brigham and Women's Hospital, Cambridge, MA, 02139, USA. j.c.h.leijten@utwente.nl; sshin4@bwh.harvard.edu; shin.lotus@gmail.com.

[⊥]These authors contributed equally to this work.

CRediT authorship contribution statement

S.R.S. conceived, designed, and coordinated the study. S.R.S., S.H., and J.L. designed, planned, and conducted in vitro and in vivo experiments, analyzed and interpreted the data, and wrote the manuscript. All the authors conducted and/or provided guidance on the experiments and read, revised, and approved the manuscript.

CRediT authorship contribution statement

Shabir Hassan: Methodology, Visualization, Investigation, Data curation, Original draft preparation, Writing-Reviewing and Editing. **Su Ryon Shin:** Conceptualization, Supervision, Methodology, Data curation, Original draft preparation, Writing-Reviewing and Editing. All the authors helped in data curation, Reviewing and Editing, and approved the manuscript.

Supporting Information

Supporting Information is available online at……..

Declaration of competing Interest

The authors declare that they have no known competing financial interests or personal relationships that could have appeared to influence the work reported in this paper

[8]Department of Biomedical Engineering, University of Illinois Chicago, Chicago IL 60612, USA.

[9]Departments of Orthopaedics, Pharmacology and Regenerative Medicine, and Mechanical and Industrial Engineering, University of Illinois Chicago, Chicago IL 60612, USA.

Abstract

Oxygenating biomaterials can alleviate anoxic stress, stimulate vascularization, and improve engraftment of cellularized implants. However, the effects of oxygen-generating materials on tissue formation have remained largely unknown. Here, we investigate the impact of calcium peroxide (CPO)-based oxygen-generating microparticles (OMPs) on the osteogenic fate of human mesenchymal stem cells (MSCs) under a severely oxygen deficient microenvironment. To this end, CPO is microencapsulated in polycaprolactone to generate OMPs with prolonged oxygen release. Gelatin methacryloyl (GelMA) hydrogels containing osteogenesis-inducing silicate nanoparticles (SNP), OMPs (OMP), or both SNP and OMP (SNP/OMP) are engineered to comparatively study their effect on the osteogenic fate of hMSCs. OMPs associate with improved osteogenic differentiation under both normoxic and anoxic conditions. Bulk RNAseq analyses suggest that OMP under anoxia regulate osteogenic differentiation pathways more strongly than SNP/OMP or SNP under either anoxia or normoxia. Subcutaneous implantations reveal a stronger host cell invasion in SNP, resulting in increased vasculogenesis. Furthermore, time-dependent expression of different osteogenic factors reveals progressive differentiation of hMSCs in OMP, SNP, and SNP/OMP hydrogels. Our work demonstrates that endowing hydrogels with OMPs can induce, improve, and steer the formation of functional engineered living tissues, which holds potential for numerous biomedical applications, including tissue regeneration and organ replacement therapy.

Graphical Abstract

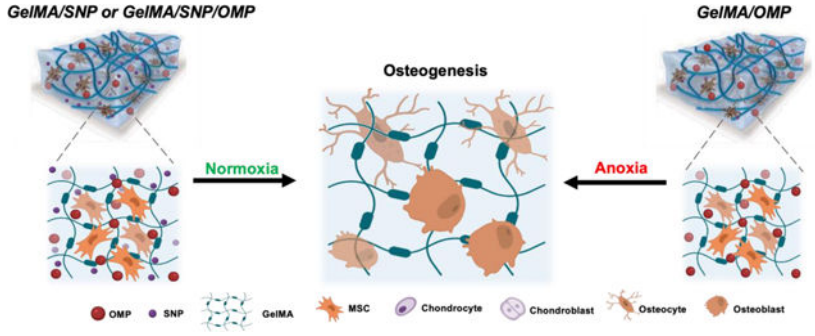

The study discusses the effect of incorporating oxygen-generating microparticles in gelatin methacryloyl hydrogels and the osteogenic differentiation fate of encapsulated human mesenchymal stem cells.

Keywords

Oxygenating materials; Stem Cell Fate; Osteogenesis; Tissue Engineering; Bone Formation

Introduction

Bone-related trauma cases in the form of critical fractures are a leading cause of physical disability and account for a significant economic burden to individuals, families, societies, and the healthcare system.[1] Current clinical therapies to treat critical fractures mostly rely on auto- or allografting.[2] Despite their limited harvest yield, autografts have remained a source of choice for bone grafts due to their low immunogenicity and excellent osteoinductive properties.[2] While bone allografts have alleviated the clinical accessibility of bone tissue, donor site morbidity and immune response have limited their use in a clinical setting.[3] Consequently, a tremendous effort has been made to develop regenerative biomaterial constructs whereby encapsulated mesenchymal stem cells (MSCs) are differentiated to osteoblasts.[4] However, controlling the oxygen tension is important for implant fate as a lower oxygen tension in known to produce articular cartilage and a higher oxygen tension associates with intramembranous ossification.[5] Specifically, oxygen not only works as a catalyst for cell metabolism and tissue regeneration, but is also required for developing new blood vessels and synthesizing collagen and other extracellular matrix components.[6] Without sufficient oxygen, tissue growth is limited, resulting in tissue death and eventually poor outcomes for tissue regeneration. Engineered control over the oxygen tension within implants can thus be considered as a potential approach to improve bone tissue engineering and regeneration.[7]

It has remained a grand challenge to bio-fabricate clinically sized bone tissue implants due to the diffusion limitation that causes oxygen and nutrient deficiency-induced cell death in the implant, which inevitably impairs its clinical efficacy.[8, 9] Before neovascularization or anastomosis, implant survival and functionality rely on passive diffusion of molecules, including oxygen, from the host.[10] Larger implants, therefore, unavoidably suffer from oxygen and nutrient diffusion constraints resulting in anoxia-induced cell death and implant failure.[11] Although various strategies, such as incorporating angiogenic growth factors with cells and bioprinting vascular constructs, have been developed to provide pre-vascularization and enable vascular anastomosis in a shortened period, the initial non-perfused phase still typically lasts for 1–2 weeks, which is ample time for implant failure. [12–15]

A recent and innovative strategy to ensure that living implants receive suitable amounts of oxygen to sustain their metabolic needs prior to being perfused is the use of oxygen-releasing biomaterials.[9, 10, 16] Compared to hyperbaric oxygen therapy[17, 18] and oxygen-carrying materials,[9, 19] oxygen-generating materials such as solid peroxides can offer more sustained and controlled oxygen release.[20–22] One of the most investigated and preferred solid inorganic peroxides, calcium peroxide (CPO), has proven to be a material of choice owing to its commercial availability and efficient, long-lasting oxygen delivery capability, especially when incorporated into a hydrophobic material. [20, 23–25] The mechanism of O_2 release of CPO involves hydrolysis-driven hydrogen peroxide (H_2O_2) formation, followed by direct decomposition of H_2O_2 into molecular oxygen.[9, 24, 26] Despite its ability to enable implant survival, empirical studies that have investigated the role of oxygen-generating materials on the functional behavior of living implants, such as

osteochondral bone defects and other disease conditions, have gained attention recently. [27, 28]

Here, we report the effect of incorporating oxygen-generating microparticles (OMP) in gelatin methacryloyl (GelMA) based osteoinductive hydrogels containing silicate nanoparticles (SNPs) on the osteogenic differentiation fate of encapsulated human MSCs (hMSCs) in particular (Schematic 1). To simulate distinct environmental conditions, engineered tissues were cultured and functionally investigated using distinct oxygen tensions (e.g., normoxia (5% O_2) to emulate optimal condition and anoxia (<0.2% O_2) to emulate severe oxygen depletion. Bulk RNA sequencing was used to dissect osteogenesis from a gene expression perspective and delineate the interplay between oxygenating materials and SNP toward hMSC fate determination for osteogenesis. Interestingly, we also observed that preconditioning of the implant in differentiating media remarkably affects cell differentiation and fate. Finally, animal studies were performed to study the expression of different genes responsible for bone formation. This study reveals that oxygen-generating materials can be used to steer the fate and functional performance of stem cells, in particular, and the osteogenic differentiation of hMSCs to improve living bone tissue implants. Most importantly, the platform can provide oxygen to the implant during the crucial prevascular phase to initiate neovascularization in the first 1–2 weeks and help the implant connect to the host tissue for transfer of oxygen and other metabolites. Based on the severity of the need, the preconditioning of the cellularized implant can be engineered to offer desired results. The freedom to tune oxygen percentage and availability time in and around a bone deficient area can be leveraged to expedite bone tissue formation.

Materials and Methods

Materials

Gelatin from porcine skin (type-A, 300 bloom; G1890), methacrylic anhydride (MW=154.16; Catalog No.: 212–084-8), polycaprolactone (PCL; MW=45,000: Catalog No.: 212–084-8), calcium peroxide (CPO; Catalog No.: 78403–22-2), goat serum (Catalog No.: G9023), calcium chloride ($CaCl_2$; Catalog No.: 10035–04-8), bovine serum albumin (BSA; Catalog No.: 9048–46-8), and Human VEGF-A ELISA Kit (Catalog No.: RAB0507–1KT) were purchased from Sigma-Aldrich (St. Louis, MO, USA) and used as received unless otherwise reported. Amplex red hydrogen peroxide assay kit (Catalog No.: A1222), Live/Dead assay kit (Catalog No.: L3224), and Human SSP1 (Osteopontin) ELISA Kit (Catalog No.: EHSPP1) were purchased from Invitrogen (USA). 2’,7’-Dichlorofluorescin Diace (DCFDA) cellular ROS detection assay kit (Catalog No.: ab113851), primary antibodies for F-actin (Catalog No.: ab205) and DAPI (Catalog No.: ab228549) were purchased from Abcam and used as per the manufacturer’s protocol. Recombinant human fibroblast growth factor basics (bFGF) was purchased from R&D Systems (Catalog No.: 4114-TC). Human HIF-1α ELISA Kit was purchased from RayBiotech (Catalog No.: ELH-HIF1a). PECAM1 (CD31; Catalog No.: P2B1) and monoclonal antibodies for macrophages (CD86; Catalog No.: MR Mab#46, CD206; Catalog No.: MR Mab#15) were purchased from Developmental Studies Hybridoma Bank (DSHB) and used as per the protocol.

Fabrication of oxygen-generating and osteoinductive GelMA hydrogels

Preparation of GelMA—High-degree methacrylation of gelatin methacryloyl (GelMA) was prepared as previously reported.[24] Briefly, 10% (w/v) of porcine Gelatin type A (Sigma-Aldrich) was dissolved in warm phosphate buffered saline (PBS) after constantly stirring (240rpm) at 50 °C until complete dissolution. To obtain a high methacryloyl substitution degree (~80%) of GelMA, 8% (v/v) methacrylic anhydride (Sigma-Aldrich) was slowly added dropwise while constantly stirring the solution mixture at 50°C for two hours. An equal volume of pre-heated (50 °C) PBS was added to the solution at the end of the duration. Subsequently, the solution mixture was dialyzed using 12–14 kDa cutoff dialysis membranes (Thermo Fisher) in de-ionized (DI) water at 40°C for at least five days. DI water was changed two times every day. On the sixth day, one volume of pre-heated (50 °C) DI water was added to the solution, followed by filtering the solution using a sterile vacuum Express Plus filtration system (0.22 μm; Millipore) and stored at −80 °C for at least two days before lyophilizing. After five-day-lyophilization, freeze-dried GelMA was obtained as a porous white foam.

Fabrication of calcium peroxide-laden polycaprolactone (CPO-PCL; OMP) microparticles OMPs were prepared using a double emulsion synthesis method of water-in-oil-in-water (w/o/w). 10% (w/v) PCL (MW=45,000, Sigma Aldrich) was dissolved in dichloromethane (DCM, Sigma Aldrich). Then, 3% (w/v) CPO (Sigma Aldrich) in DI water was added to the PCL solution. This was followed by emulsification using ultrasonication (QSonica) for two min at 60% amplitude with a two sec ON and one sec OFF pulse mode (Emulsion 1). Subsequently, the processed solution was mixed into prepared 1% gelatin solution on ice and ultrasonicated at 60% amplitude for an extra four min without a pulse (Emulsion 2). After ultrasonication, the solution was stirred in a hood overnight to evaporate DCM at room temperature. The particles were collected through centrifugation of the solution (Eppendorf 5702, Germany) at 5,000 rpm for 20 min. The microparticles pellet was rinsed with methanol and ethanol twice to remove adhesive residual additives. Finally, microparticle pellets were washed with DI water three times, after which the microparticle pellets were frozen with liquid nitrogen and dried by freezedryer for 4–5 days. For the control group (0% CPO-PCL), microparticles were prepared by the above-mentioned protocol without adding CPO.

Fabrication of nanocomposite-GelMA hydrogels

For nanocomposite-GelMA hydrogels, different concentrations of OMPs or SNPs (w/v) were added to a 2% GelMA-PBS solution. Before adding to the pre-gel solution, OMPs and SNPs were sterilized under UV exposure of 2–5 mins inside a biosafety cabinet. The mixture solution was bath sonicated for two min at room temperature. Subsequently, 7.5% (w/v) GelMA was obtained by supplementing the remaining weight of GelMA, and 0.25% (w/v) photoinitiator (Irgacure) was added to all the solutions for photocrosslinking. 50 μl of respective solution was added between two 1-mm-thickness glass slides and covered by a coverslip. To obtain cylindrical crosslinked hydrogels, the GelMA pre-polymer solutions with respective materials were exposed to UV light for 25 seconds at 800 mW/cm^2, placed at 8 cm from the UV source (OmniCure S2000, Excelitas USA).

Structural, mechanical, and degradation characterization of nanocomposite hydrogels

Scanning electron microscopy (SEM) imaging—To analyze the crosslinked porous structure of nanocomposite-GelMA hydrogels, SEM (Supra55; Zeiss) was used. The as-fabricated samples were flash-frozen in liquid nitrogen, followed by lyophilization for at least two days. The lyophilized hydrogel samples were broken to expose their cross-sections. The samples were then sputter coated with gold using a sputter coater (Cressington 106 Auto Sputter Coater). Samples were imaged under accelerating voltages of 3–10kV.

Mechanical testing—To measure compressive strength under changed strain values and to determine Young's modulus of the crosslinked nanocomposite-hydrogels, OMP, SNP, and SNP/OMP hydrogels of different concentrations of SNP, OMP, and SNP/OMP, respectively, were loaded onto an Instron 5944 mechanical tester. The hydrogels were applied with a compressive strain at 0.5 mm/min strain rate up to 50% deformation at room temperature. Young's moduli were calculated from the linear region of the curve ranging between 10 to 15% strain of the stress-strain curve. Each measurement was carried out for five samples in each group.

Oxygen release kinetics—400 μL of OMP, SNP, and SNP/OMP nanocomposite-hydrogels were individually placed inside a cryovial with 600 μL of anoxic PBS. For a two-point calibration of the Opto-F1 Uni-Amp optic oxygen sensor (Unisense), one sample of PBS was bubbled with air, and another sample (anoxic) was obtained by bubbling nitrogen gas for 10 minutes inside an anoxic glove box. Microparticles were put in anoxic PBS before a calibrated measurement. Dissolved oxygen was recorded using the Unisense senor. Measurements were performed daily for 14 days.

Quantification of hydrogen peroxide (H_2O_2) release kinetics—H_2O_2 generation was detected using the Amplex red hydrogen peroxide assay kit (Invitrogen, Thermo Fisher) according to the manufacturer's protocol. Each hydrogel sample was placed individually in a tube containing 1 mL PBS and the lip of the tube was tightly sealed by parafilm to prevent evaporation at room temperature. 10 μL of supernatant from each sample was collected daily, and the sample was replenished with an equal volume of PBS. After diluting the supernatant with PBS, the H2O2 assay was performed in a total volume of 100 μL per microplate well and eventually evaluated using a 96-well-plate reader (SpectraMax i3; Molecular Devices).

In vitro degradation behavior of nanocomposite GelMA hydrogels—The assessment of crosslinked hydrogels for their degradation profiles was performed based on our previous study[29] to mimic the accelerated enzymatic degradation of these biomaterials in vivo. First, OMP, SNP, and SNP/OMP nanocomposite hydrogel samples with different concentrations of OMP and SNP were prepared as discs of 8mm width and 1 mm thickness. Next, each hydrogel was put in the 1.5 ml tube with 1ml PBS solution for three hours before enzymatic degradation experiments. Collagenase type II solution at a concentration of 3.278 mg/mL was freshly prepared, and resultant solutions with different hydrogels and collagenase concentrations were incubated. This concentration for collagenase type II was chosen based on our previous studies on the in vitro biodegradation of GelMA hydrogels.

[24, 25] Samples were removed from the enzyme-containing solutions at 0h, 6h, 12h, 24h, and 36h, washed with PBS, weighed, lyophilized, and weighed again after lyophilization.

hMSC culture and encapsulation in nanocomposite hydrogels—hMSCs were obtained from Lonza Bioscience (Catalog#: PT-2501) and seeded in low glucose-DMEM growth medium containing 10% fetal bovine serum, 1% penicillin streptomycin (P/S; Thermo Fisher Scientific) and 10 ng/mL recombinant human fibroblast growth factor basics (bFGF; R&D, Systems). Cells were grown to 80% confluency (approximately five days). A medium change was performed 24 hours before harvest. The medium was aspirated from the vessel on the day of harvest, followed by a gentle washing with 1x DPBS (Corning). Cells were harvested by gently distributing 0.025% trypsin and 0.01% EDTA in DPBS. To harvest, the harvest solution was gently distributed throughout the vessels for one minute before being incubated at 37°C until the cells dislodged. The solution was collected after an equivalent volume of growth media was used to liberate cells from the growing surface. Cells were pooled, and cell concentration and viability checked with trypan blue followed by centrifugation at 600 x g for 5–10 minutes. Concentrated cell suspension was then resuspended in new medium. Cells at a required number and between passages 4–6 were cultured in the same way and used for all experiments. To prepare cell-laden nanocomposite hydrogels, trypsinized hMSCs were suspended in a 7.5% (w/v) GelMA prepolymer solution containing different concentrations (w/v %) of SNP and OMP with a cell density of 3×10^6 cells/mL. Pre-polymer hydrogel solutions were then photocrosslinked to form hydrogels using UV exposure as described in earlier. Non-crosslinked pre-polymer components were removed by washing the fabricated cell-laden hydrogels in normal media and cultured in normal growth medium under normoxic (21% O_2, 5% CO_2, and 74% N_2) and hypoxic (1% O_2, 5% CO_2, and 94% N_2) conditions before following experiments.

In vitro 3D osteogenic differentiation of hMSCs in nanocomposite hydrogels—The osteogenic differentiation of encapsulated hMSCs was induced in the osteoinductive medium, which was prepared by supplementing high glucose-DMEM media with 50 μg/mL-ascorbic acid (Wako), 10 mM β-glycerophosphate (EMD Millipore), and 100 nM dexamethasone (MP biomedicals). Unless otherwise reported, the normal growth medium was replaced after seven days with the osteoinductive medium in differentiation groups. Cell culture media of both the control group and differentiation group were changed every third day during the experimental period.

In vitro cytocompatibility studies with nanocomposite-GelMA hydrogels—The cells were studied for cytocompatibility and other characterizations under different environmental conditions. Severe hypoxic conditions were maintained using a commercial BioSpherix Hypoxia System (Biospherix Ltd. USA). Cell viability was determined by staining hMSCs within the hydrogel using a Live/Dead assay kit (Invitrogen, USA) according to the manufacturer's instructions. Cells encapsulated in hydrogels were stained with calcein AM (0.5 μL/mL) and ethidium homodimer-1 (EthD-1, 2 μL/mL) in PBS. The cells were incubated at 37 °C for 45 min, followed by PBS washing three times to remove the remaining staining solutions thoroughly. Subsequently, samples were observed and imaged under an inverted fluorescence microscope (Olympus, Japan). Fiji Image J

software was used to count the number of living (green fluorescence) and dead cells (red fluorescence). Cell viability was calculated as a ratio of live cells to dead cells. Cell viability (%) = (living cell numbers /total cell numbers) x 100. To assess cell spreading in hydrogels, Fiji Image J was used to count the number of elongated cells. Cell elongation (%) = (elongated cell numbers /total cell numbers) x 100.

Alkaline phosphatase (ALP) activity—The ALP activity was measured using a colorimetric assay (Alkaline Phosphatase Assay Kit, ab83369) following the standard procedure, which quantifies the conversion of p-nitrophenol phosphate (pNPP) to colored p-Nitrophenol (pNP) when dephosphorylated by ALP. Cultured hydrogels were washed with PBS at each endpoint and lysed with ALP assay buffer after homogenization. Cell lysate and 5 mM pNPP solution were added to a 96-well plate and protected from light. After one hour of incubation at 25°C, the absorbance at 405 nm was measured on a microplate reader (SpectraMax i3, Molecular Devices). A standard curve was made by adding ALP enzyme solution to pNPP standards solution (0–20 nM), and ALP activity (μmol/min/mL) in each sample was calculated from the standard curve. To obtain comparable ALP activity (μmol/min/μg of DNA), quantitation of double-stranded DNA (dsDNA) in samples was determined using a PicoGreen dsDNA Quantification Kit (P7589, Invitrogen, Molecular Probes, USA). Cell lysate and PicoGreen assay reagent were added to a 96-well plate and incubated in the dark for five min at RT. The fluorescence of samples was measured using a microplate reader (SpectraMax i3, Molecular Devices) at excitation ~480 nm and emission at ~520 nm. DNA concentration (μg/mL) of the sample was calculated from generated DNA standard curve using a DNA standard. ALP was reported as normalized to the total DNA content of the cells.

Alizarin Red S staining—Cells encapsulated in hydrogels were first fixed with 4% Paraformaldehyde (PFA) in PBS solution for 20 min at room temperature (RT, 24 °C) and then washed with DI water three times to remove all traces of PFA and salt residues. The fixed cells were then covered with 2% (wt/v) Alizarin Red S solution (ARS, Sigma Aldrich, Germany) in DI water at an adjusted pH range of 4.1–4.3. After staining for two min at RT, cells were washed with DI water and then imaged using an inverted optical microscope (Olympus, Japan). To quantify calcium deposition, the stained constructs were incubated overnight in 10% acetic acid (Sigma Aldrich, Germany). The collected solution was centrifuged at 20,000 g for 15 minutes, and the supernatant was transferred to other tubes and neutralized with the same volume of 10% NH_4OH (Sigma Aldrich, Germany). 100 μL of each sample in a 96-well plate was analyzed at 405 nm using a microplate reader (SpectraMax i3, Molecular Devices).

Immunostaining—After culturing for 21 days, cells encapsulated in nanocomposite OMP, SNP, and SNP/OMP hydrogels were first washed with PBS and fixed in 4% PFA for 20 min at RT. The hydrogels were then treated with 0.1% Triton X in PBS for one hour to permeabilize the cells at RT. 10% goat serum was used as a blocking solution for one hour at RT. The hydrogels were then incubated with the following primary antibodies: mouse monoclonal anti-human osteocalcin (1: 200) or mouse monoclonal anti-human osteopontin (1: 200), in 10% goat serum overnight at 4 °C. Next day, the constructs were treated with

secondary antibody: Alexa Fluor 594 goat anti-mouse (1: 500) or Alexa Fluor 488 goat anti-mouse (1: 500), for one hour at RT. The constructs were then counterstained with diamidino-2-phenyindole dilactate (DAPI) for five min to stain nuclei. Between each step, hydrogels were washed three times with PBS for 10 min each. Finally, immunofluorescence microscopy of the obtained samples was conducted using a confocal microscope (Zeiss, LSM880, Germany).

Real-time quantitative PCR—Real-time quantitative PCR (qPCR) was used to assess the levels of OPN and OCN mRNA following the incubation of cell-laden nanocomposite OMP, SNP, and SNP/OMP hydrogels with growth or osteoinductive medium for 21 days. The following primer sequences were synthesized by Integrated DNA Technologies (USA) and used for qPCR, including OPN (F: 5'-CTCAGGCCAGTTGCAGCC-3' and R:5'- CAAAAGCAAATCACTG CAATTCTC-3'), OCN (F: 5'- TCACACTCCTCGCCCTATTG-3' and R: 5'- TCGCTGCCCT CCTGCTTG-3') and GADPH (F: 5'- AAGGTGAAGGTCGGAGTCAAC-3' and R: 5'-GGG GTCATTGATGGCAACAATA-3'). The relative mRNA level of target genes and control GAPDH was calculated using the 2-ΔΔC(t) method. The ratio of target genes to GADPH was normalized with that from pristine GelMA hydrogel cultured in a normal growth medium.

RNA-Seq—mRNA was isolated from hMSCs in nanocomposite OMP, SNP, and SNP/OMP hydrogels cultured under anoxia or normoxia conditions on days 0, 14, and 28 using TRIzol (Invitrogen) following the manufacturer's protocol. Samples that qualified QC on a bioanalyzer (with an RNA Integrity Number (RIN) score of > 8) were subjected to mRNA enrichment using oligo (dT) beads. rRNA was depleted using Illumina Ribo-zero kit followed by fragmentation and cDNA synthesis using random hexamers. After second strand synthesis using custom second-strand synthesis Illumina kit sequencing adapters were ligated. Finally, the library was size selected, and PCR enriched. Pooled library was loaded to Illumina sequencer to its effective 4 nM concentration.

QC was done on 150 bp FASTQ paired end reads generated per sample. Adapter sequences and reads below the Phred score of Q30 were trimmed. For all the samples, more than 95% of reads qualify the Q30 threshold, indicating very high-quality data. Finally, all FASTQ files were analyzed for any bias via MultiQC. All samples showed consistent 50% GC content and passed QC. Using splicing aware STAR aligner (STAR_2.5.0a), reads were aligned to human genome build hg19 with parameters "--runMode alignReads --outSAMtype BAM SortedByCoordinate --outSAMattributes Standard --outSAMunmapped Within --quantMode GeneCounts". We were able to map more than 90% of reads per sample. Alignment quality control was performed using qualimap (QualiMap v.2.2.1), and all alignments passed QC. Gene counts table generated from STAR was used to generate a linear model in DESeq2 as "design = ~Condition + Treatment + Time + Condition:Treatment + Condition:Time + Treatment:Time". To generate differentially regulated genes, the contrast level was set either between normoxia and anoxia within the same day or across different time points. To identify the gene signature of OMP, SNP, and SNP/OMP, the levels were contrasted per time point within normoxia or anoxia by setting

only GelMA as a reference sample. To explore the underlying gene regulatory modules for each contrast, an unbiased gene set enrichment analysis (GSEA) was performed using KEGG and REACTOME pathway genes. A cutoff of adjusted p-value < 0.05 and absolute normalized enrichment score > 2 was used to prioritize the signaling pathways in each condition. RNAseq data are available on public repository (BioProject ID PRJNA953747) and can be accessed here: http://www.ncbi.nlm.nih.gov/bioproject/953747

In vivo study

Biodegradation and biocompatibility of composite hydrogels in vivo—The biodegradation and biocompatibility of the nanocomposite OMP, SNP, and SNP/OMP hydrogels were evaluated subcutaneously in rats. All animal procedures were approved by the Institutional Animal Use and Care Committee of Harvard Medical School (Protocol number: 2017N000114). 8-week-old Sprague Dawley rats were acclimatized in the vivarium of Brigham and Women's Hospital for a week prior to surgery. 3mm x 8mm cylindrical nanocomposite hydrogel samples with different concentrations of OMP and SNP were prepared and cultured in a medium overnight before surgery. A subcutaneous space was accessed through a dorsal incision on the backs after the rats were anesthetized with isoflurane. Subsequently, four hydrogel samples per rat were introduced into the subcutaneous pockets on the bilateral sides of the cut. Carprofen (5 mg/kg BW/day s.c.) was postoperatively administered for three days to alleviate post-surgery pain of the animals. One week and three weeks post-surgery, the implanted hydrogels and surrounding tissue of each group were harvested for further immunological response study. The harvested samples were fixed in 4% paraformaldehyde and stained with Hematoxylin and Eosin (H&E), CD31 antibody, CD86 antibody, and CD206 antibody after paraffin embedding.

Bone deposition of hMSCs laden nanocomposite hydrogels in vivo—Nude rats (RNU) were used to study the biodegradation and bone deposition of hMSCs-laden nanocomposite hydrogels by subcutaneous implantation. All animals were used after approval for all procedures from Harvard Medical School's Institutional Animal Use and Care Committee (Protocol number: 2017N000114). Before surgery, nude rats (8-week-old) were acclimatized for a week in the vivarium of Brigham and Women's Hospital. Firstly, hMSC-encapsulated nanocomposite hydrogel samples with 3mm thickness and 8mm diameter were prepared and cultured in a normal growth medium or osteoinductive differentiation medium at different times. Subsequently, they were subcutaneously implanted on the backs of nude rats (RNU) as described in 4.10.1. 4 samples were embedded in one rat and 3 samples were tested for each group. To alleviate post-surgery pain of rats, carprofen (5 mg/kg BW/day s.c.) was postoperatively administered for three days. Four weeks after the surgery, the implanted hMSC-laden hydrogels and surrounding tissue of each group were harvested and fixed in 4% paraformaldehyde for further immumohistochemical and immunofluorescence analysis, such as HE staining, collagen I, HIF-1α, Aggrecan, and CD31 expression study.

Statistical analyses

For significance, all experiments were repeated in triplicate. The obtained data are expressed as means ± SD. The significance was studied using a two-tailed t-test (Student's unpaired

t-test) for two-group comparisons, and for multiple groups, one-way analysis of variance (ANOVA) with Dunnett's posttest was used. To evaluate the differences between groups involving change over time, we performed ANOVA test with repeated measures.

Results and Discussion

Fabrication and characterization of oxygenating and osteoinductive hydrogels

To evaluate the effect of oxygen on osteoinductive hydrogels, three different nanocomposite hydrogels were fabricated with GelMA hydrogels containing OMP, SNP, or both OMP and SNP. OMPs were synthesized using a double-emulsion method previously described in our protocol.[24, 25] The synthesized OMPs showed a size distribution of 4.2 ± 1.7 μm (Figure 1A and Supplementary Figure S1A). To generate a homogenous particle dispersion in the high concentration of GelMA pre-polymer solution (Supplementary Figure S1B), OMPs were sonicated in 2% GelMA pre-polymer solution for 2 mins. In previous studies, GelMA, which contains ~40% hydrophobic amino acids, was used as a bio-surfactant to disperse hydrophobic nanoparticles, such as carbon nanotube and graphene.[30, 31] Using a similar approach, the amphiphilic GelMA chains were coated on the surface of hydrophobic OMPs via the hydrophobic amino acids, while hydrophilic amino acids on GelMA chains interacted with the adjacent water phase. This allowed for OMPs to be homogeneously dispersed in the high concentration of GelMA hydrogels with minimal aggregation at different concentrations. SNP nanoclay (nanodiscs) of 25 ± 10 nm diameter and 1–5 nm thickness were incorporated in the OMP-laden GelMA hydrogels to endow the hydrogels with osteoinductive properties, as previously reported.[32–34]

The addition of SNP and OMP (PCL), which are stiffer materials (~MPa range)[35, 36] than GelMA hydrogels (~few tens kPa),[37, 38] might increase the stiffness of the nanocomposite hydrogels as compared to pristine GelMA hydrogel. Enhanced mechanical properties have been shown to improve nucleation of cell-secreted calcium and overall enhance osteogenic differentiation of hMSCs in vitro.[39–42] Also, calcium peroxide (CPO) in the OMP affects crosslinking of OMP because of free radical formation from CPO hydrolysis and less UV absorption due to opacity from OMPs compared to the transparent hydrogel as in pristine GelMA.[24, 25] To compensate for these differences, the UV exposure times were fine-tuned in order to endow all hydrogels with comparable mechanical properties. This normalization minimized the effect of mechanical stiffness of hydrogels, thus allowing a more unbiased focus on the functional impact of OMP and SNP on hMSC differentiation. Analysis of the mechanical test results confirmed that hydrogels were characterized by compressive moduli of 45–55 kPa (Figure 1B). The compressive stress at breakpoints for all the groups was observed to be between 75–95 kPa corresponding to 40–55% strain (Supplementary Figure S1C, D). It is noteworthy that the bulk properties of hydrogels may not reveal the perspective of mechanical forces at a cellular level; as such, we performed nanoindentation studies on hydrogels with SNPs (Supplementary Figure S1E). SNPs at 0.1% considerably increased the Young's modulus of the hydrogels compared to 0.05% and 0.025%, where there was no significant increase. Morphology of the OMP, SNP, and SNP/OMP nanocomposite hydrogels was characterized by SEM. Of note, the microporous structures of three hydrogels taken by a SEM do not reflect the in-situ pore structure,

but rather the collapsed pore structure following freeze-drying. Nevertheless, this form of SEM analysis offers a good prediction of the pore size variation [24, 25, 43] All hydrogels maintained microporous structures similar to that of pristine GelMA hydrogels (Figure 1C), and OMPs were well embedded in the GelMA matrix. As shown in Figure 1D, the average pore size was mildly increased when incorporating OMPs into the hydrogel. This observation could potentially be explained by the release of oxygen during photo-initiated crosslinking. Indeed, the observed mild differences in pore sizes were positively correlated with the degradation rate of the various hydrogels (Figure 1E).

An interesting and surprising oxygen release behavior was observed in SNP/OMP hydrogels, which showed <0.2 μM oxygen release after four days of incubation (Figure 1F). SNPs have been shown to play a role in the sequestration of gases and have been used to produce oxygen-enriched microenvironments due to their adsorption properties.[44–47] Based on our observation, it could be anticipated that some of the oxygen released by OMPs is therefore sequestered by the SNPs. Since nanoporous silica has been shown to degrade >80% in 4 weeks under in vitro conditions,[48] we believe the sequestered oxygen will again become available following SNP degradation, thus effectively altering the oxygen release profile. In contrast, OMP was characterized by prolonged oxygen release following an anticipated curve with ~0.31 μM for 14 days, which was similar to our previous studies. [24, 25] H_2O_2 was released as an intermediate in the hydrolysis of CPO during oxygen generation (Supplementary Equation 1,2).[22, 24, 25] Unrestrained hydrolysis of CPO is associated with the generation of H_2O_2 levels that are known to be detrimental to cell survival.[49, 50] Encapsulating CPO within biocompatible and hydrophobic PCL limited the hydrolytic rate of CPO, which resulted in cytocompatible levels of H_2O_2 by keeping the concentration under a few dozen micromoles, which is sufficiently low so as not to cause oxidative DNA lesions of cells.[51] The released amounts of H_2O_2 levels declined progressively over a period of two weeks. Compared to pristine GelMA hydrogels, the H_2O_2 released levels were below 30 μM even for the highest OMP concentrations used (Figure 1G).

Viability of hMSCs in oxygen-generating and osteoinductive hydrogels

The effect of OMPs and SNPs on the viability and proliferation of encapsulated hMSCs in OMP, SNP, and SNP/OMP was investigated in the growth medium for two weeks under normoxia and anoxia (Figure 2). To this end, the formulation of OMPs for generating enough oxygen and the concentration of SNPs for improving osteogenesis were studied, and the apparent optimal formulation was selected. Various concentrations of OMPs (e.g., CPO in PCL microparticles) ranging from 0–3% were investigated under normoxic conditions on cell survival (Figure 2, Supplementary Figure S2). GelMA hydrogels encapsulating OMPs up to 0.5% maintained high cell viability, which was in agreement with our recent study that also showed that 0.25% OMPs consisting of 3% CPO released sufficient molecular oxygen in two weeks to support the physiological demand.[25]

Beyond OMP concentration, osteoinductive SNPs can potentially also exert cytotoxicity due to their degradation into toxic silanol groups, which can initiate intracellular oxidative stress or lead to DNA damage (genotoxicity).[48] To find an optimal concentration of SNP for

high cell viability and osteogenesis, we prepared hMSC-laden SNP hydrogels with various concertation of SNPs under normoxic and anoxic conditions (Supplementary Figure S3). At 0.05% SNP under normoxia, the SNP hydrogels demonstrated either similar or higher viability than those at 0.025% and 0.1% concentrations of SNP, respectively (Figure 2A, C, Supplementary Figure S3A). At these concentrations of SNP, cells in SNP showed a decline in their viability from around 90% to below 80% on days 1 and 4, respectively. However, on day 10, the cells showed considerable recovery, with more than 90% of cells viable and proliferating (Supplementary Figure S3B). In contrast, SNP under anoxic condition revealed a constant cell death rate for all concentrations of SNP as the study progressed with cell viability going below 50% on day 10 (Figure 2B, D, Supplementary Figure S3). It is pertinent to mention that OMP presence could not completely rescue the cell death due to oxidative stress or genotoxicity induced by SNPs under different conditions.[48] Consequently, for all the future experiments in this paper, SNP and OMP concentrations for OMP, SNP, and SNP/OMP were used at 0.05%, and 0.1–0.25%, respectively. Notably, anoxic cultures associated with a decrease in cell survival as compared to normoxic cultures, owing to anoxia-induced cell death, whereby cellular viability was rescued in OMP and SNP/OMP due to OMP-driven alleviation of anoxia.

We next studied the effect of OMPs in hMSC-laden SNP hydrogels on cell viability under two different oxygen concentrations. Interestingly, under normoxic condition, OMP and SNP/OMP with 0.25% OMPs decreased the viability of the hMSCs by about 10% on day 1 compared with other groups (Figure 2 A,C). This might be due to the hydrolysis of the CPO nanocrystals decorated on the outer surface of the OMPs, causing a burst release of a high concentration of H_2O_2 (~25 μM) during the first 24 hours.[24, 25] The viability from the 0.25% OMP-containing groups increased in the following days and matched that of the pristine GelMA control group. Surprisingly, when cultured in an anoxic environment, the SNP group was characterized by a considerable amount of cell death as compared to the pristine GelMA control group. This indicated that SNPs could possess a previously unidentified cytotoxic nature when used under anoxic conditions. In contrast, two OMP-laden groups maintained their viability ~90% up to 10 days under anoxic condition, thus suggesting that the presence of OMPs negated the cytotoxic effects of both anoxia and SNPs (Figure 2C,D). Furthermore, the results are supported by the cell proliferation measurements, as depicted by the percentage of elongated cells present (Figure 2E).

Osteogenic differentiation in oxygenating and osteoinductive hydrogels

We next studied the effect of SNP/OMP hydrogels on the osteogenic differentiation of hMSC, as determined by the normalized activity of alkaline phosphatase (ALP) as a marker of early osteogenic differentiation under normoxic and anoxic conditions for up to 21 days. ALP expression progressively increased in all samples when cells were cultured under normoxic conditions (Figure 3A). In contrast, anoxia negatively influenced ALP activity (Figure 3B). SNPs in the SNP group inhibited ALP expression, which was most likely caused by the reduction in cellular viability (Supplementary Figure S4A). Importantly, supplementing SNPs with OMPs not only rescued the inhibition of ALP expression but consistently resulted in the highest ALP expression. This observation was corroborated by OPN and OCN immunohistochemical staining (Supplementary Figure S4B–D), which

revealed that the addition of OMP to pristine hydrogel or SNP constructs substantially increases their expression (Figure 3C–F). Similarly, gene expression analysis (qRT-PCR) confirmed that expression of *OCN* and *OPN* was highest in SNP/OMP constructs, especially when composed of 0.05% SNPs and 0.1% OMP (Figure 3G).

We then studied the matrix mineralization of the engineered hydrogels by visualizing the deposited calcium after four weeks of anoxic or normoxic culture. It is interesting to note that all calcium deposition levels were similar, except for the SNP group (Figure 3H,I). While SNP showed an increased calcium deposition under normoxia, when cells were cultured under an anoxic condition, the SNP constructs did not show such a trend (Supplementary Figure S4E,F). Together, these studies complement the role of OMPs in SNP/OMP, initiating the differentiation of hMSCs toward osteoblast formation as depicted by calcium mineralization. Surprisingly, OMP constructs increased hydrogel calcifications efficiently under normoxic and anoxic conditions, suggesting a potential pro-osteogenic effect of OMPs. It is pertinent to mention that although extrinsic supplementation of Ca^{2+} has shown to affect MSC differentiation into osteoblasts,[52–54] the concentrations of CPO used in this study release 10–20 times Ca^{2+} to affect their commitment. As such, the stimulation toward osteoblast differentiation is driven by oxygen, and not calcium hydroxide.

Mechanical analysis complemented the observed improvements in osteogenesis in terms of compressive strength, with the SNP/OMP nanocomposite hydrogels showing the highest moduli under both normoxic and anoxic culture (Figure 3J,K). Specifically, after seven days in proliferation medium or 28 days cultured in a normoxic or anoxic microenvironment, the only condition that consistently was characterized by a significantly higher compressive modulus as compared to pristine GelMA hydrogel were SNP/OMP constructs containing 0.05% SNP and 0.25% OMP. This could be due to a combinatorial effect from OMPs and SNPs when present in the highest tested concentrations. Individually, both SNPs and OMPs have been shown to increase the mechanical strength of hydrogels.[24, 55] When exposing the engineered hydrogels to seven days of proliferation medium followed by 28 days of osteogenic differentiation medium, OMP as well as SNP/OMP constructs were characterized by an increase in the mechanical strength. This corroborates with a detected increase in extracellular matrix deposition, jointly indicating that OMPs stimulate osteogenic differentiation and rescue the SNP function under anoxic conditions.[56]

Role of oxygenation in orchestrating osteogenic differentiation fate of hMSCs encapsulated living hydrogels

While the incorporation of nanocomposite materials such as silicates and oxalates can enhance osteogenic differentiation through their mechanical and mineralization properties,[4, 42, 57] oxygen gradients can also potentially guide stem cell fate toward osteogenesis.[58–60] To dissect whether there is a combinatorial effect on the osteogenic fate of hMSCs in our systems, we performed a bulk mRNA sequence analysis of hMSCs encapsulated in OMP, SNP, or SNP/OMP constructs. Specifically, genes and gene profiles responsible for osteogenesis of hMSC encapsulated in GelMA hydrogels containing OMP (0.25%) and/or SNP (0.05%) cultured under normoxia or anoxia in an osteogenic differentiation

medium for up to 28 days were studied. A global analysis showed gene expression under anoxia, represented as red dots in Fig. 4, was enhanced overall, as compared to in normoxic conditions, represented in turquoise (Figure 4A). This iis in line with published literature.[61] While initially both conditions did not show much difference in the gene expression profiles as depicted from PC1, a prolonged exposure in osteogenic differentiation media for two and four weeks shows very distinct variation in the expression profiles in both conditions. Looking closely at the influence from different hydrogels, particularly on osteogenic initiation, the groups result in a mixed response in gene expression profiles under normoxia (Supplementary Figure S5A); however, SNP/OMP under anoxia results in a higher change in the expression profiles after 28 days compared to other groups (Supplementary Figure S5B). Among the remaining groups under anoxia, OMP results in an increased expression towards osteogenesis at 14 and 28 days. GelMA and SNP do not show much difference in PC1 compared to PC2. Overall, anoxia positively impacted hMSCs fitness and transcriptome, potentially improving inherent properties over time for the important molecular pathways that may be important in osteogenesis.

It has been shown that oxygen partial pressure and hypoxic culture conditions influence signaling pathways, amongst others, via HIF1A and HIF2A, which can regulate cellular differentiation, metabolism, and apoptosis.[62–64] As expected, anoxia enhanced the overall HIF1A expression in samples with OMP compared to SNP and SNP/OMP, indicating that the difference in oxygen tension was sensed in all conditions (Figure 4B). Furthermore, no major differences in HIF1A expression were observed between the OMP, SNP, and SNP/OMP conditions indicating similar and stable behavior for this gene at the transcriptional level between conditions with comparable oxygen tensions. We then analyzed these gene sets with the Molecular Signatures Database (MsigDB) using the DESeq2 tool and revealed that pathways involving cytokine production, vasculogenesis, microtubule-based movement, and osteoblast differentiation were differentially expressed. Most importantly, and in line with our previous observations, both OMP and SNP/OMP were positively correlated with the gene sets relating to osteoblast differentiation when comparing anoxia and normoxia (Figure 4D). This corroborated the positive effect of OMPs on osteogenic differentiation of hMSCs under anoxic conditions. Detailed analysis of the most relevant differentially regulated genes was performed for pristine, SNP, OMP, and SNP/OMP constructs cultured under normoxia (Figure 4E) and anoxia (Figure 4F) for 14 days. Expression levels of genes relevant for osteogenesis (Supplementary Information) were revealed to be distinct between hydrogel compositions.

Notably, OMPs showed an upregulation of *BMP6*, *ATF4*, *CTNNB1*, *HES1*, and *DDX21* in anoxia. BMP6 has been shown to activate ALP activity via Smad1 and Smad5.[65] Similarly, HES1 activates RUNX2 via pRB interaction for osteogenesis.[66] CTNNB1 has been shown to promote proliferation and osteoblastogenesis of hMSCs via Wnt/β-catenin pathway. Interestingly, SNP constructs stimulated hMSCs to transcribe *COL10A*, which is a known marker for the hypertrophic differentiation phase of chondrogenesis. Regardless, the upregulation of these genes in the OMP constructs, especially under anoxic conditions, indicated the promotion of osteogenesis by the self-oxygenating hydrogels. This suggested that modulation of local oxygen tension using self-oxygenating hydrogels has the potential

to orchestrate the differentiation of hMSCs toward osteogenesis and engineer living tissues for bone defects and injuries in regenerative medicine.

Biocompatibility, biodegradation, and neovascularization of oxygenating hydrogels

To empirically validate the in vivo biocompatibility and long-term immune response, 150 mm^3 (8 mm wide and 3 mm thick) acellular pristine GelMA (Group 1), OMP (0.25% OMP; Group 2), SNP (0.05% SNP; Group 3), and SNP/OMP (0.05% SNP + 0.25% OMP; Group 4) hydrogels were subcutaneously implanted on the backs of Sprague-Dawley rats (Figure 5A). The hydrogels were explanted after 1 and 3 weeks, representing short- and long-term immune responses, and analyzed for biodegradation, host cell infiltration, and neovascularization. To examine biodegradation and host–graft interaction, midsagittal slices of the explants were histologically and immunologically evaluated. Staining with hematoxylin and eosin (H&E) (Figure 5B), CD31 for neovascularization, and CD86/206 for host immune cell infiltration verified slower degradation, lesser neovascularization, and showed less presence of cells in the core of pristine GelMA constructs, even after three weeks of implantation (Figure 5A, B).

H&E staining revealed that biodegradation and hydrogel resorption was more prominent three weeks post-implantation in all the experimental groups as compared to one-week post-implantation. Interestingly, OMP constructs were associated with significantly more rapid biodegradation than all other samples, including SNP/OMP. Possibly this could be explained by the observation that OMPs were more porous than other formulations. Increased porosity allows for altered degradation profiles, more expedient diffusion of (catabolic) enzymes, and more rapid infiltration of host cells. Similar to previously published results, native GelMA hydrogels and those containing only PCL particles (no CPO) were characterized by a significantly slower degradation rate than the corresponding composite hydrogels with OMPs.[24] This resulted in increased cell proliferation, CD31+ expression, and vascularization than the other control groups. Regardless, this indicated that OMPs not only guide cell fate, but also the implant’s fate by controlling the construct’s degradation rate. These results corroborate to the in vitro degradation of OMP and SNP/OMP hydrogels, as reported in Figure 1E, which are fast-paced as compared to the pristine GelMA hydrogels. The encapsulated cells deposit matrix that affects the mechanical properties of these hydrogels as shown in Figure 3J,K. The degradation rate also inversely correlated with the ingrowth of CD31+ cells (Figure 5C) as well as vessel diameter (Figure 5D). OMPs thus can contribute to implant vascularization, possibly by controlling the degradation rate. Surprisingly, although OMP possessed larger vessels, the SNP/OMP condition was characterized by the highest number of vessels, albeit typically smaller vessels (Figure 5E). This could possibly be explained by the observation that the SNPs in the SNP construct also mildly stimulated the number of (small) vessels. The SNP constructs were also associated with a considerable increase in CD86+ cells, indicating a host immune response via macrophage infiltration, which was mitigated by the incorporation of OMPs as observed in the SNP/OMP constructs (Figure 5F). No significant differences were observed for CD206+ cells for any of the construct formulations (Figure 5G). Taken together, these results suggest that OMPs can act in a pro-angiogenic manner that does not elicit an elevated immune response upon implantation.

Role of pre-differentiation duration in vitro on the osteochondral fate of SNP/OMP hydrogels in vivo

We next set out to study the effect on osteogenesis and tissue formation in vivo using hMSC-laden hydrogels. In addition, the effect of in vitro preculture was studied to gain further understanding and the potential relevance of in vitro pretreatment on implant fate. Importantly, we studied the effect of OMPs (Supplementary Figure S6) versus the effect of pretreatment duration (Supplementary Figure S7) on the osteogenesis of MSCs in vivo. Based on our results, osteogenic hydrogels containing 0.05% SNP with or without 0.25% OMP were studied. Moreover, all groups were cultured for one week in the proliferation medium, followed either by 0, 1, or 2 weeks of exposure to the osteogenic differentiation medium. The temporal investigation on implanting scaffolds composed of gradually differentiating hMSCs indicated osteoinduction was not needed for improved osteogenic differentiation (Supplementary Information).

Conclusion

In conclusion, we report that endowing biomaterials with self-oxygenating properties can promote the osteogenic fate of encapsulated hMSCs. We investigated hydrogel scaffolds reinforced with OMPs for their oxygen releasing capabilities and their influence on driving osteogenesis in vitro and in vivo under different environmental conditions. A comparison of effects of OMPs with and without an osteoinductive mineral, SNP, was made for studying mechanical resilience of the scaffolds, cell survival, and expression of several bone development markers under normoxic and anoxic conditions. In vitro, OMPs alone showed higher levels of cell survival and proliferation, but SNP addition resulted in higher ALP activity. Bulk RNA studies revealed that OMPs induced a more osteogenic gene transcript fingerprint than SNPs or SNPs and OMPs combined. In vivo, self-oxygenation of biomaterials demonstrated a greater host cell invasion that correlated with enhanced vasculogenesis. Additional studies are needed to fully unravel the exact roles of these biomaterials in different osteogenic differentiation pathways. Regardless, the results from this study reflect on the role of oxygenating biomaterials toward osteogenesis for regenerative medicine applications required under oxygen-deprived circumstances such as bone and muscle tissue scaffolds.

Supplementary Material

Refer to Web version on PubMed Central for supplementary material.

Acknowledgements

This work was jointly supported by the National Institutes of Health (R01AR074234), AHA Innovative Project Award (19IPLOI34660079), and the Gillian Reny Stepping Strong Center for Trauma Innovation at Brigham and Women's Hospital to SRS. JL acknowledges financial support from the European Research Council (ERC, Starting Grant, 759425) and Health-Holland (LSHM19074).

REFERENCES

[1]. Wu A-M, Bisignano C, James SL, Abady GG, Abedi A, Abu-Gharbieh E, Alhassan RK, Alipour V, Arabloo J, Asaad M, Asmare WN, Awedew AF, Banach M, Banerjee SK, Bijani A, Birhanu

TTM, Bolla SR, Cámera LA, Chang J-C, Cho DY, Chung MT, Couto RAS, Dai X, Dandona L, Dandona R, Farzadfar F, Filip I, Fischer F, Fomenkov AA, Gill TK, Gupta B, Haagsma JA, Haj-Mirzaian A, Hamidi S, Hay SI, Ilic IM, Ilic MD, Ivers RQ, Jürisson M, Kalhor R, Kanchan T, Kavetskyy T, Khalilov R, Khan EA, Khan M, Kneib CJ, Krishnamoorthy V, Kumar GA, Kumar N, Lalloo R, Lasrado S, Lim SS, Liu Z, Manafi A, Manafi N, Menezes RG, Meretoja TJ, Miazgowski B, Miller TR, Mohammad Y, Mohammadian-Hafshejani A, Mokdad AH, Murray CJL, Naderi M, Naimzada MD, Nayak VC, Nguyen CT, Nikbakhsh R, Olagunju AT, Otstavnov N, Otstavnov SS, Padubidri JR, Pereira J, Pham HQ, Pinheiro M, Polinder S, Pourchamani H, Rabiee N, Radfar A, Rahman MHU, Rawaf DL, Rawaf S, Saeb MR, Samy AM, Sanchez Riera L, Schwebel DC, Shahabi S, Shaikh MA, Soheili A, Tabarés-Seisdedos R, Tovani-Palone MR, Tran BX, Travillian RS, Valdez PR, Vasankari TJ, Velazquez DZ, Venketasubramanian N, Vu GT, Zhang Z-J, Vos T, Global, regional, and national burden of bone fractures in 204 countries and territories, 1990–2019: a systematic analysis from the Global Burden of Disease Study 2019, The Lancet Healthy Longevity 2(9) (2021) e580–e592. [PubMed: 34723233]

[2]. Baldwin P, Li DJ, Auston DA, Mir HS, Yoon RS, Koval KJ, Autograft, Allograft, and Bone Graft Substitutes: Clinical Evidence and Indications for Use in the Setting of Orthopaedic Trauma Surgery, J Orthop Trauma 33(4) (2019) 203–213. [PubMed: 30633080]

[3]. Sohn H-S, Oh J-K, Review of bone graft and bone substitutes with an emphasis on fracture surgeries, Biomaterials Research 23(1) (2019) 9. [PubMed: 30915231]

[4]. Stamnitz S, Klimczak A, Mesenchymal Stem Cells, Bioactive Factors, and Scaffolds in Bone Repair: From Research Perspectives to Clinical Practice, Cells 10(8) (2021).

[5]. Leijten J, Georgi N, Moreira Teixeira L, van Blitterswijk CA, Post JN, Karperien M, Metabolic programming of mesenchymal stromal cells by oxygen tension directs chondrogenic cell fate, Proceedings of the National Academy of Sciences 111(38) (2014) 13954–13959.

[6]. Yamada S, Yassin MA, Weigel T, Schmitz T, Hansmann J, Mustafa K, Surface activation with oxygen plasma promotes osteogenesis with enhanced extracellular matrix formation in three-dimensional microporous scaffolds, Journal of Biomedical Materials Research Part A 109(9) (2021) 1560–1574. [PubMed: 33675166]

[7]. Hannah SS, McFadden S, McNeilly A, McClean C, “Take My Bone Away?” Hypoxia and bone: A narrative review, Journal of Cellular Physiology 236(2) (2021) 721–740. [PubMed: 32643217]

[8]. Gholipourmalekabadi M, Zhao S, Harrison BS, Mozafari M, Seifalian AM, Oxygen-generating biomaterials: a new, viable paradigm for tissue engineering?, Trends in biotechnology 34(12) (2016) 1010–1021. [PubMed: 27325423]

[9]. Willemen NG, Hassan S, Gurian M, Li J, Allijn IE, Shin SR, Leijten J, Oxygen-Releasing Biomaterials: Current Challenges and Future Applications, Trends in biotechnology (2021).

[10]. Touri M, Moztarzadeh F, Abu Osman NA, Dehghan MM, Brouki Milan P, Farzad-Mohajeri S, Mozafari M, Oxygen-releasing scaffolds for accelerated bone regeneration, ACS Biomaterials Science & Engineering 6(5) (2020) 2985–2994.

[11]. McMurtrey RJ, Analytic Models of Oxygen and Nutrient Diffusion, Metabolism Dynamics, and Architecture Optimization in Three-Dimensional Tissue Constructs with Applications and Insights in Cerebral Organoids, Tissue Eng Part C Methods 22(3) (2016) 221–49. [PubMed: 26650970]

[12]. Laschke MW, Menger MD, Prevascularization in tissue engineering: current concepts and future directions, Biotechnology advances 34(2) (2016) 112–121. [PubMed: 26674312]

[13]. Rouwkema J, Rivron NC, van Blitterswijk CA, Vascularization in tissue engineering, Trends in biotechnology 26(8) (2008) 434–441. [PubMed: 18585808]

[14]. Zhu W, Qu X, Zhu J, Ma X, Patel S, Liu J, Wang P, Lai CSE, Gou M, Xu Y, Direct 3D bioprinting of prevascularized tissue constructs with complex microarchitecture, Biomaterials 124 (2017) 106–115. [PubMed: 28192772]

[15]. Kérourédan O, Hakobyan D, Rémy M, Ziane S, Dusserre N, Fricain J-C, Delmond S, Thébaud NB, Devillard R, In situ prevascularization designed by laser-assisted bioprinting: effect on bone regeneration, Biofabrication 11(4) (2019) 045002.

[16]. Kim HY, Kim SY, Lee H-Y, Lee JH, Rho G-J, Lee H-J, Lee H-C, Byun J-H, Oh SH, Oxygen-Releasing Microparticles for Cell Survival and Differentiation Ability under Hypoxia

for Effective Bone Regeneration, Biomacromolecules 20(2) (2019) 1087–1097. [PubMed: 30642156]

[17]. Plafki C, Peters P, Almeling M, Welslau W, Busch R, Complications and side effects of hyperbaric oxygen therapy, Aviation Space and Environmental Medicine 71(2) (2000) 119–124. [PubMed: 10685584]

[18]. Lam G, Fontaine R, Ross FL, Chiu ES, Hyperbaric oxygen therapy: exploring the clinical evidence, Advances in skin & wound care 30(4) (2017) 181–190. [PubMed: 28301358]

[19]. Liu Y, Zhao X, Zhao C, Zhang H, Zhao Y, Responsive porous microcarriers with controllable oxygen delivery for wound healing, Small 15(21) (2019) 1901254.

[20]. Suvarnapathaki S, Wu X, Lantigua D, Nguyen MA, Camci-Unal G, Breathing life into engineered tissues using oxygen-releasing biomaterials, NPG Asia Materials 11(1) (2019) 1–18.

[21]. Suvarnapathaki S, Nguyen MA, Goulopoulos AA, Lantigua D, Camci-Unal G, Engineering calcium peroxide based oxygen generating scaffolds for tissue survival, Biomaterials Science 9(7) (2021) 2519–2532. [PubMed: 33565527]

[22]. Willemen NGA, Hassan S, Gurian M, Li J, Allijn IE, Shin SR, Leijten J, OxygenReleasing Biomaterials: Current Challenges and Future Applications, Trends in Biotechnology 39(11) (2021) 1144–1159. [PubMed: 33602609]

[23]. Aleemardani M, Solouk A, Akbari S, Dehghan MM, Moeini M, Silk-derived oxygen-generating electrospun patches for enhancing tissue regeneration: investigation of calcium peroxide role and its effects on controlled oxygen delivery, Materialia 14 (2020) 100877.

[24]. Farzin A, Hassan S, Teixeira LSM, Gurian M, Crispim JF, Manhas V, Carlier A, Bae H, Geris L, Noshadi I, Shin SR, Leijten J, Self-Oxygenation of Tissues Orchestrates Full-Thickness Vascularization of Living Implants, Adv Funct Mater 31(42) (2021).

[[25]]. Willemen NGA, Hassan S, Gurian M, Jasso-Salazar MF, Fan K, Wang H, Becker M, Allijn IE, Bal-Ozturk A, Leijten J, Shin SR, Enzyme-mediated Alleviation of Peroxide Toxicity in Self-oxygenating Biomaterials, Adv Healthc Mater (2022) e2102697.

[26]. Burg KJ, Porter S, Kellam JF, Biomaterial developments for bone tissue engineering, Biomaterials 21(23) (2000) 2347–2359. [PubMed: 11055282]

[27]. Suvarnapathaki S, Nguyen A, Goulopoulos A, Camci-Unal G, Oxygen-Generating Scaffolds for Cardiac Tissue Engineering Applications, ACS Biomater Sci Eng 9(1) (2023) 409–426. [PubMed: 36469567]

[28]. Mandal K, Sangabathuni S, Haghniaz R, Kawakita S, Mecwan M, Nakayama A, Zhang C, Edalati M, Huang W, Lopez AH, Jucaud V, Dokmeci MR, Khademhosseini A, Oxygen-generating microparticles downregulate HIF-1α expression, increase cardiac contractility, and mitigate ischemic injury, Acta Biomaterialia (2023).

[29]. Siebert L, Luna-Cerón E, García-Rivera LE, Oh J, Jang J, Rosas-Gómez DA, Pérez-Gómez MD, Maschkowitz G, Fickenscher H, Oceguera-Cuevas D, Light-Controlled Growth Factors Release on Tetrapodal ZnO-Incorporated 3D-Printed Hydrogels for Developing Smart Wound Scaffold, Advanced Functional Materials 31(22) (2021) 2007555.

[30]. Shin SR, Bae H, Cha JM, Mun JY, Chen Y-C, Tekin H, Shin H, Zarabi S, Dokmeci MR, Tang S, Khademhosseini A, Carbon Nanotube Reinforced Hybrid Microgels as Scaffold Materials for Cell Encapsulation, ACS Nano 6(1) (2012) 362–372. [PubMed: 22117858]

[31]. Shin SR, Jung SM, Zalabany M, Kim K, Zorlutuna P, Kim S.b., Nikkhah M, Khabiry M, Azize M, Kong J, Wan K.-t., Palacios T, Dokmeci MR, Bae HX Tang A Khademhosseini, Carbon-Nanotube-Embedded Hydrogel Sheets for Engineering Cardiac Constructs and Bioactuators, ACS Nano 7(3) (2013) 2369–2380. [PubMed: 23363247]

[32]. Junior CRF, Fernandes R.d.S., Moura M, Aouada FA, HYDROPHILIC AND KINETIC PROPERTIES OF NANOCLAY LAPONITE RDS AND POLY (METHACRYLIC ACID) (PMAA) HYDROGEL NANOCOMPOSITES, 2018.

[33]. Afghah F, Altunbek M, Dikyol C, Koc B, Preparation and characterization of nanoclay-hydrogel composite support-bath for bioprinting of complex structures, Scientific Reports 10(1) (2020) 5257.

[34]. Martín-Moldes Z, López Barreiro D, Buehler MJ, Kaplan DL, Effect of the silica nanoparticle size on the osteoinduction of biomineralized silk-silica nanocomposites, Acta Biomaterialia 120 (2021) 203–212. [PubMed: 33160114]

[35]. Dwivedi R, Kumar S, Pandey R, Mahajan A, Nandana D, Katti DS, Mehrotra D, Polycaprolactone as biomaterial for bone scaffolds: Review of literature, J Oral Biol Craniofac Res 10(1) (2020) 381–388. [PubMed: 31754598]

[36]. Liff SM, Kumar N, McKinley GH, High-performance elastomeric nanocomposites via solvent-exchange processing, Nature Materials 6(1) (2007) 76–83. [PubMed: 17173034]

[37]. Yue K, Trujillo-de Santiago G, Alvarez MM, Tamayol A, Annabi N, Khademhosseini A, Synthesis, properties, and biomedical applications of gelatin methacryloyl (GelMA) hydrogels, Biomaterials 73 (2015) 254–271. [PubMed: 26414409]

[38]. Zhu M, Wang Y, Ferracci G, Zheng J, Cho N-J, Lee BH, Gelatin methacryloyl and its hydrogels with an exceptional degree of controllability and batch-to-batch consistency, Scientific Reports 9(1) (2019) 6863. [PubMed: 31053756]

[39]. Antebi B, Cheng X, Harris JN, Gower LB, Chen XD, Ling J, Biomimetic collagenhydroxyapatite composite fabricated via a novel perfusion-flow mineralization technique, Tissue Eng Part C Methods 19(7) (2013) 487–96. [PubMed: 23157544]

[40]. Vissers CA, Harvestine JN, Leach JK, Pore size regulates mesenchymal stem cell response to Bioglass-loaded composite scaffolds, Journal of Materials Chemistry B 3(44) (2015) 8650–8658. [PubMed: 32262722]

[41]. Koons GL, Diba M, Mikos AG, Materials design for bone-tissue engineering, Nature Reviews Materials 5(8) (2020) 584–603.

[42]. Wu X, Zhang T, Hoff B, Suvarnapathaki S, Lantigua D, McCarthy C, Wu B, Camci-Unal G, Mineralized Hydrogels Induce Bone Regeneration in Critical Size Cranial Defects, Adv Healthc Mater 10(4) (2021) e2001101.

[43]. Gombert Y, Roncoroni F, Sánchez-Ferrer A, Spencer ND, The hierarchical bulk molecular structure of poly(acrylamide) hydrogels: beyond the fishing net, Soft Matter 16(42) (2020) 9789–9798. [PubMed: 33001127]

[44]. Lian M, Xue Z, Qiao X, Liu C, Zhang S, Li X, Huang C, Song Q, Yang W, Chen X, Wang T, Movable Hollow Nanoparticles as Reactive Oxygen Scavengers, Chem 5(9) (2019) 2378–2387.

[45]. Sibag M, Choi B-G, Suh C, Lee KH, Lee JW, Maeng SK, Cho J, Inhibition of total oxygen uptake by silica nanoparticles in activated sludge, Journal of Hazardous Materials 283 (2015) 841–846. [PubMed: 25464327]

[46]. Cuko A, Bromley ST, Calatayud M, Oxygen Vacancies in Oxide Nanoclusters: When Silica Is More Reducible Than Titania, Frontiers in Chemistry 7 (2019).

[47]. Tiwari D, Kaur S, Bhunia H, Bajpai PK, CO2 adsorption on oxygen enriched nanostructured carbons derived from silica templated resorcinol-formaldehyde, Journal of Industrial and Engineering Chemistry 65 (2018) 146–155.

[48]. Hadipour Moghaddam SP, Mohammadpour R, Ghandehari H, In vitro and in vivo evaluation of degradation, toxicity, biodistribution, and clearance of silica nanoparticles as a function of size, porosity, density, and composition, J Control Release 311-312 (2019) 1–15.

[49]. Giorgio M, Trinei M, Migliaccio E, Pelicci PG, Hydrogen peroxide: a metabolic by-product or a common mediator of ageing signals?, Nature Reviews Molecular Cell Biology 8(9) (2007) 722–728. [PubMed: 17700625]

[50]. Barbieri E, Sestili P, Reactive Oxygen Species in Skeletal Muscle Signaling, Journal of Signal Transduction 2012 (2012) 982794.

[51]. Nakamura J, Purvis ER, Swenberg JA, Micromolar concentrations of hydrogen peroxide induce oxidative DNA lesions more efficiently than millimolar concentrations in mammalian cells, Nucleic Acids Res 31(6) (2003) 1790–1795. [PubMed: 12626721]

[52]. Kon E, Muraglia A, Corsi A, Bianco P, Marcacci M, Martin I, Boyde A, Ruspantini I, Chistolini P, Rocca M, Giardino R, Cancedda R, Quarto R, Autologous bone marrow stromal cells loaded onto porous hydroxyapatite ceramic accelerate bone repair in critical-size defects of sheep long bones, J Biomed Mater Res 49(3) (2000) 328–37. [PubMed: 10602065]

[53]. Cheng S, Wang W, Lin Z, Zhou P, Zhang X, Zhang W, Chen Q, Kou D, Ying X, Shen Y, Cheng X, Yu Z, Peng L, Lu C, Effects of extracellular calcium on viability and osteogenic differentiation of bone marrow stromal cells in vitro, Human Cell 26(3) (2013) 114–120. [PubMed: 23749732]

[54]. Lee MN, Hwang H-S, Oh S-H, Roshanzadeh A, Kim J-W, Song JH, Kim E-S,Koh TJ, Elevated extracellular calcium ions promote proliferation and migration of mesenchymal stem cells via increasing osteopontin expression, Experimental & Molecular Medicine 50(11) (2018) 1–16.

[55]. Kim C, Lee JW, Heo JH, Park C, Kim D-H, Yi GS, Kang HC, Jung HS, Shin H, Lee JH, Natural bone-mimicking nanopore-incorporated hydroxyapatite scaffolds for enhanced bone tissue regeneration, Biomaterials Research 26(1) (2022) 7.

[56]. Liao X, Lu S, Zhuo Y, Winter C, Xu W, Li B, Wang Y, Bone Physiology, Biomaterial and the Effect of Mechanical/Physical Microenvironment on MSC Osteogenesis: A Tribute to Shu Chien's 80th Birthday, Cell Mol Bioeng 4(4) (2011) 579–590. [PubMed: 25580165]

[57]. Wu X, Gauntlett O, Zhang T, Suvarnapathaki S, McCarthy C, Wu B, Camci-Unal G, Eggshell Microparticle Reinforced Scaffolds for Regeneration of Critical Sized Cranial Defects, ACS Applied Materials & Interfaces 13(51) (2021) 60921–60932. [PubMed: 34905346]

[58]. Merceron C, Vinatier C, Portron S, Masson M, Amiaud J, Guigand L, Chérel Y, Weiss P, Guicheux J, Differential effects of hypoxia on osteochondrogenic potential of human adipose-derived stem cells, Am J Physiol Cell Physiol 298(2) (2010) C355–64. [PubMed: 19940068]

[59]. O'Reilly A, Kelly DJ, Role of oxygen as a regulator of stem cell fate during the spontaneous repair of osteochondral defects, J Orthop Res 34(6) (2016) 1026–36. [PubMed: 26595173]

[60]. Mohyeldin A, Garzón-Muvdi T, Quiñones-Hinojosa A, Oxygen in stem cell biology: a critical component of the stem cell niche, Cell Stem Cell 7(2) (2010) 150–61. [PubMed: 20682444]

[61]. Elabd C, Ichim TE, Miller K, Anneling A, Grinstein V, Vargas V, Silva FJ, Comparing atmospheric and hypoxic cultured mesenchymal stem cell transcriptome: implication for stem cell therapies targeting intervertebral discs, Journal of Translational Medicine 16(1) (2018) 222.

[62]. Choi JR, Pingguan-Murphy B, Abas WABW, Azmi MAN, Omar SZ, Chua KH, Safwani WKZW, Impact of low oxygen tension on stemness, proliferation and differentiation potential of human adipose-derived stem cells, Biochemical and biophysical research communications 448(2) (2014) 218–224. [PubMed: 24785372]

[63]. Påhlman S, Mohlin S, Hypoxia and hypoxia-inducible factors in neuroblastoma, Cell and Tissue Research 372(2) (2018) 269–275. [PubMed: 29032465]

[64]. Heyman SN, Leibowitz D, Mor-Yosef Levi I, Liberman A, Eisenkraft A, Alcalai R, Khamaisi M, Rosenberger C, Adaptive response to hypoxia and remote ischaemia pre-conditioning: a new hypoxia-inducible factors era in clinical medicine, Acta Physiologica 216(4) (2016) 395–406. [PubMed: 26449466]

[65]. Aoki H, Fujii M, Imamura T, Yagi K, Takehara K, Kato M, Miyazono K, Synergistic effects of different bone morphogenetic protein type I receptors on alkaline phosphatase induction, J Cell Sci 114(Pt 8) (2001) 1483–9. [PubMed: 11282024]

[66]. Lee JS, Thomas DM, Gutierrez G, Carty SA, Yanagawa S, Hinds PW, HES1 cooperates with pRb to activate RUNX2-dependent transcription, J Bone Miner Res 21(6) (2006) 921–33. [PubMed: 16753023]

[67]. Morimoto D, Kuroda S, Kizawa T, Nomura K, Higuchi C, Yoshikawa H, Tomita T, Equivalent osteoblastic differentiation function of human mesenchymal stem cells from rheumatoid arthritis in comparison with osteoarthritis, Rheumatology (Oxford) 48(6) (2009) 643–9. [PubMed: 19398485]

[68]. Rafalski VA, Mancini E, Brunet A, Energy metabolism and energy-sensing pathways in mammalian embryonic and adult stem cell fate, J Cell Sci 125(Pt 23) (2012) 5597–608. [PubMed: 23420198]

[69]. Tiaden AN, Breiden M, Mirsaidi A, Weber FA, Bahrenberg G, Glanz S, Cinelli P, Ehrmann M, Richards PJ, Human serine protease HTRA1 positively regulates osteogenesis of human bone marrow-derived mesenchymal stem cells and mineralization of differentiating bone-forming cells through the modulation of extracellular matrix protein, Stem Cells 30(10) (2012) 2271–82. [PubMed: 22865667]

[70]. Bruderer M, Richards RG, Alini M, Stoddart MJ, Role and regulation of RUNX2 in osteogenesis, Eur Cell Mater 28 (2014) 269–86. [PubMed: 25340806]

[71]. Toh WS, Guo X-M, Choo AB, Lu K, Lee EH, Cao T, Differentiation and enrichment of expandable chondrogenic cells from human embryonic stem cells in vitro, J Cell Mol Med 13(9B) (2009) 3570–3590.

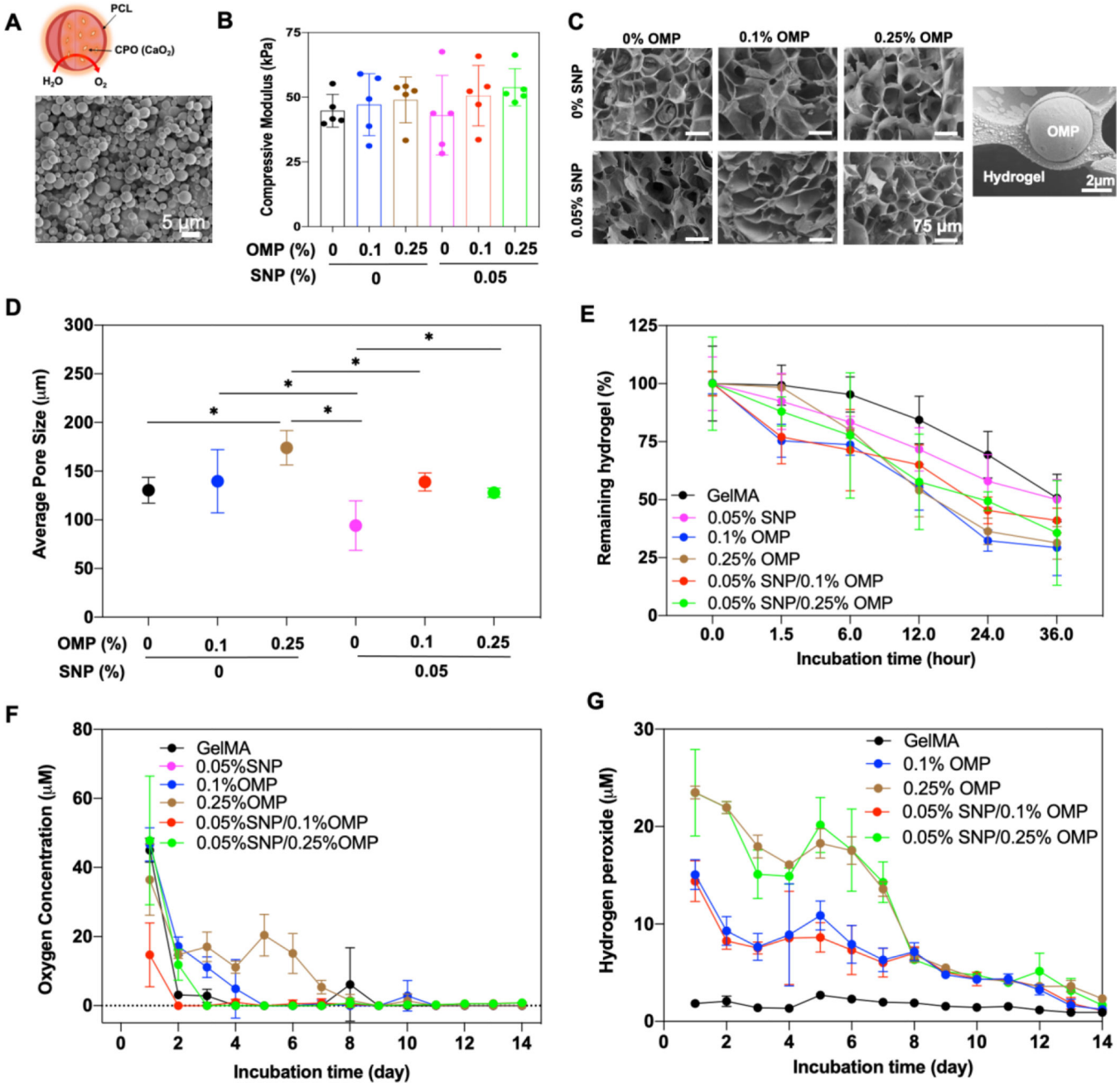

Figure 1: Material characterization of oxygenating and osteoinductive nanocomposite hydrogels.

(A) SEM image of the synthesized OMPs. (**B**) Compressive modulus (n=3) and (**C**) SEM images of nanocomposite GelMA hydrogels reinforced with OMP, SNP, and both OMP/SNP particles. An SEM image of OMP microparticle in GelMA hydrogel is also shown. Pore size quantification of the engineered nanocomposite hydrogels from **C**. (n=3; *p<0.05). Enzymatic degradation of nanocomposite hydrogels is affected by the integration of OMP, SNP, and their combination (n=3). (**F**) Oxygen and **(G)** H_2O_2 release kinetics of nanocomposite hydrogels reinforced with various concentration of OMP, 0.05% SNP, and their combination (n=3; *p<0.05).

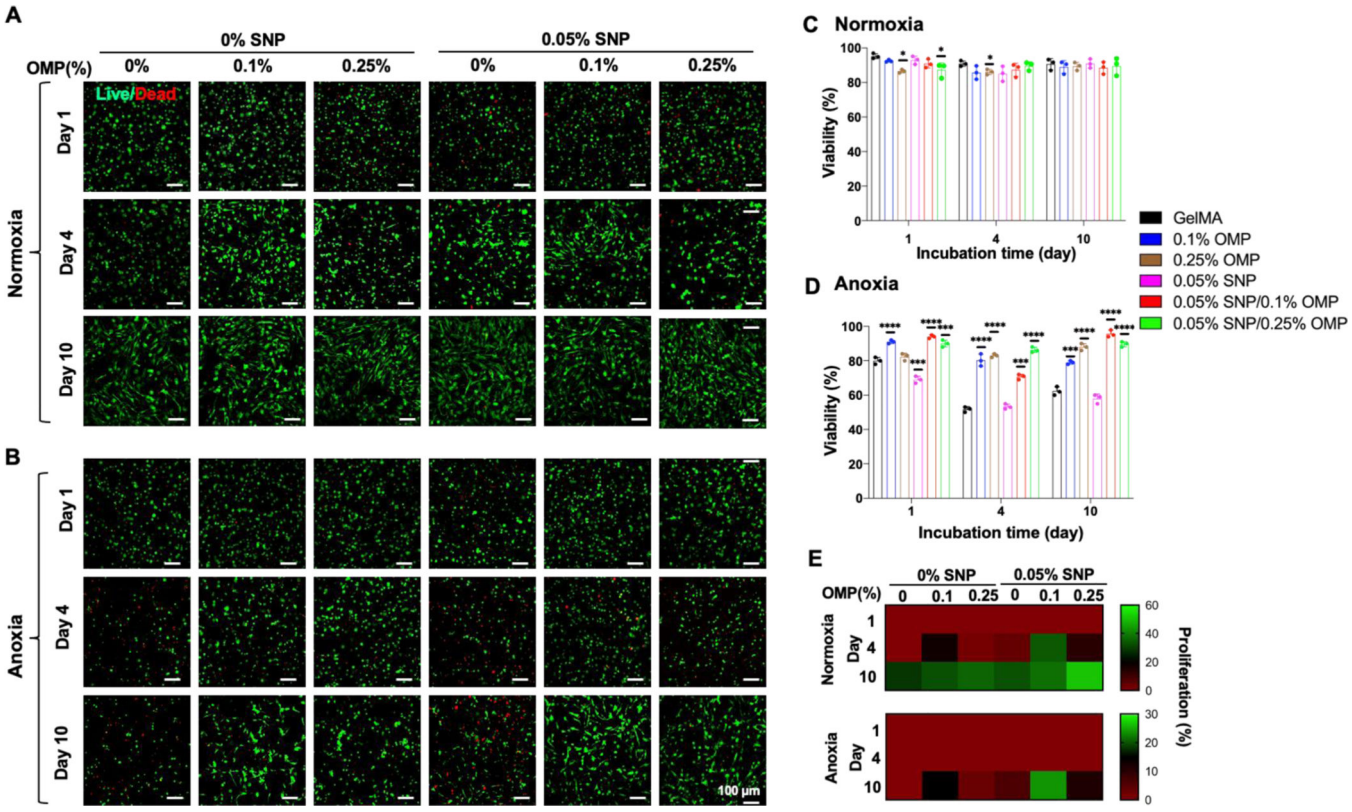

Figure 2: Viability of hMSCs encapsulated in OMP, SNP, and SNP/OMP nanocomposite GelMA hydrogels.

(A, B) Live/Dead images of hMSCs encapsulated in GelMA nanocomposite hydrogels with different concentrations of SNPs and OMPs under (**A**) normoxic and (**B**) anoxic conditions for ten days. (**C**, **D**) Quantitative analysis of viability for hMSCs in (**A**) and (**B**), respectively. (n=3; *p<0.05). (**E**) Proliferation studies of hMSCs in 0.05% SNP-laden GelMA nanocomposite hydrogels with different concentration of OMPs (0, 0.1, and 0.25%) under normoxic and anoxic. The scale bar represents 100 μm. (n=3; ****p<0.0001).

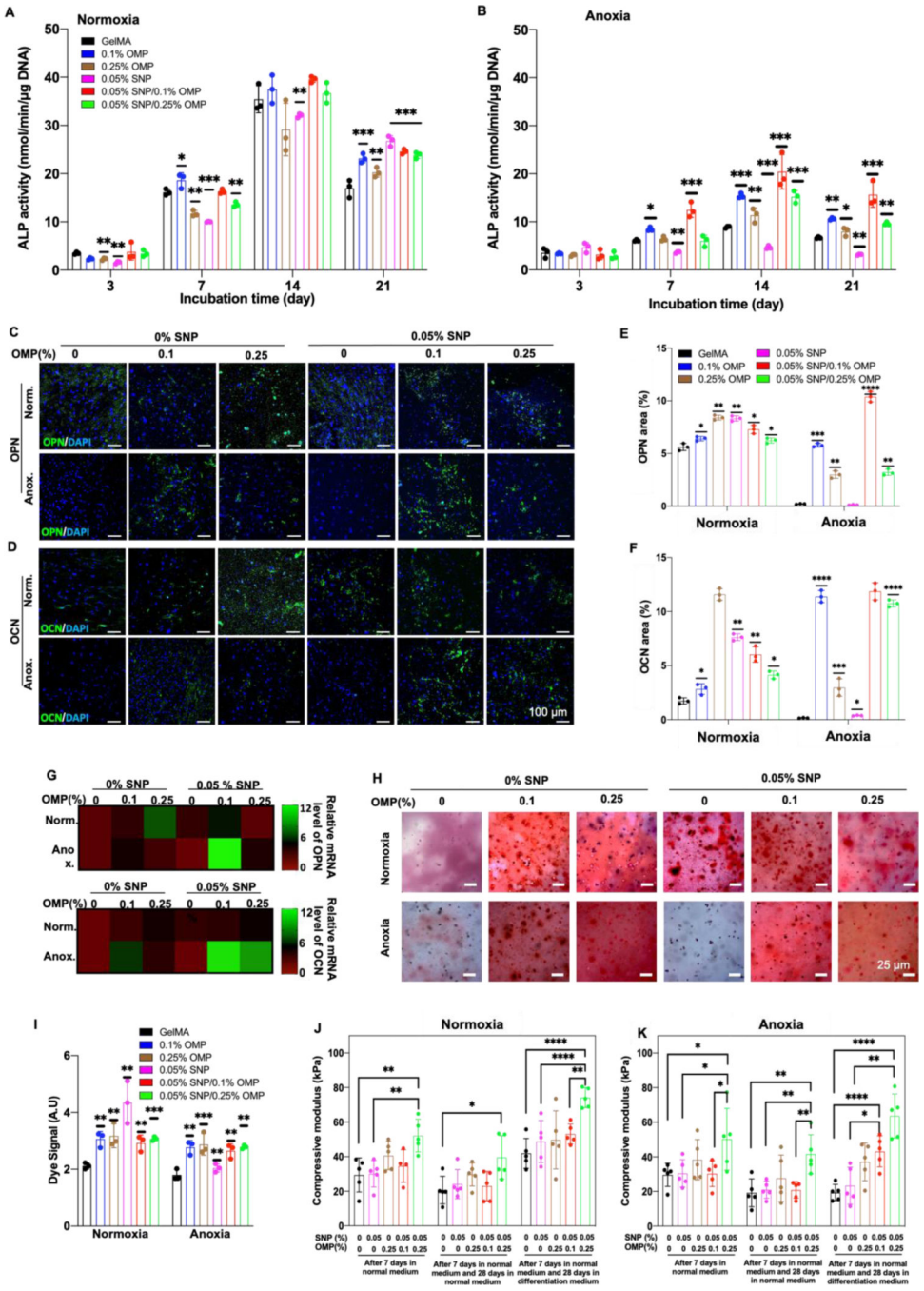

Figure 3: Osteogenic differentiation of hMSCs encapsulated in oxygen-generating and/or osteoinductive hydrogels with different concentration of SNPs and OMPs under normoxia and anoxia.

(A,B) ALP activity normalized to the total amount of DNA of encapsulated hMSCs in pristine, OMP, SNP, or SNP/OMP constructs under (**A**) normoxia and (**B**) anoxia. (n=3; ****p<0.0001, ***p<0.001, **p<0.01, *p<0.05). (**C**,**D**) Fluorescence microphotographs and (**E**,**F**) associated semi-quantitative image analysis of hMSC-laden hydrogels immunohistochemically stained for OPN and OCN after being cultured in osteogenic differentiation media under normoxic or anoxic conditions. (**G**) QRT-PCR analysis for

three relative mRNA expression levels of late osteogenic markers *OPN* and *OCN* from hMSCs encapsulated in pristine, OMP, SNP, and SNP/OMP hydrogels after being cultured under normoxic or anoxic conditions in osteogenic differentiation media for three weeks. (n=3; ****p<0.0001, ***p<0.001, **p<0.01, *p<0.05). (**H**) Microphotographs and (**I**) semi-quantitative image analysis of Alizarin red stained hMSC-laden hydrogels after being cultured in osteogenic differentiation media under normoxic or anoxic conditions for 28 days. (n=3; ***p<0.001, **p<0.01). The compressive modulus of hMSC-laden in pristine OMP, SNP, and SNP/OMP hydrogels for either 7 or 35 days using distinct temporal exposure to proliferation and osteogenic differentiation media under (**J**) normoxic or (**K**) anoxic conditions. Scale bar (**C**) = 25 μm, (**H**) = 100 μm. (n=3; ****p<0.0001, **p<0.01, *p<0.05).

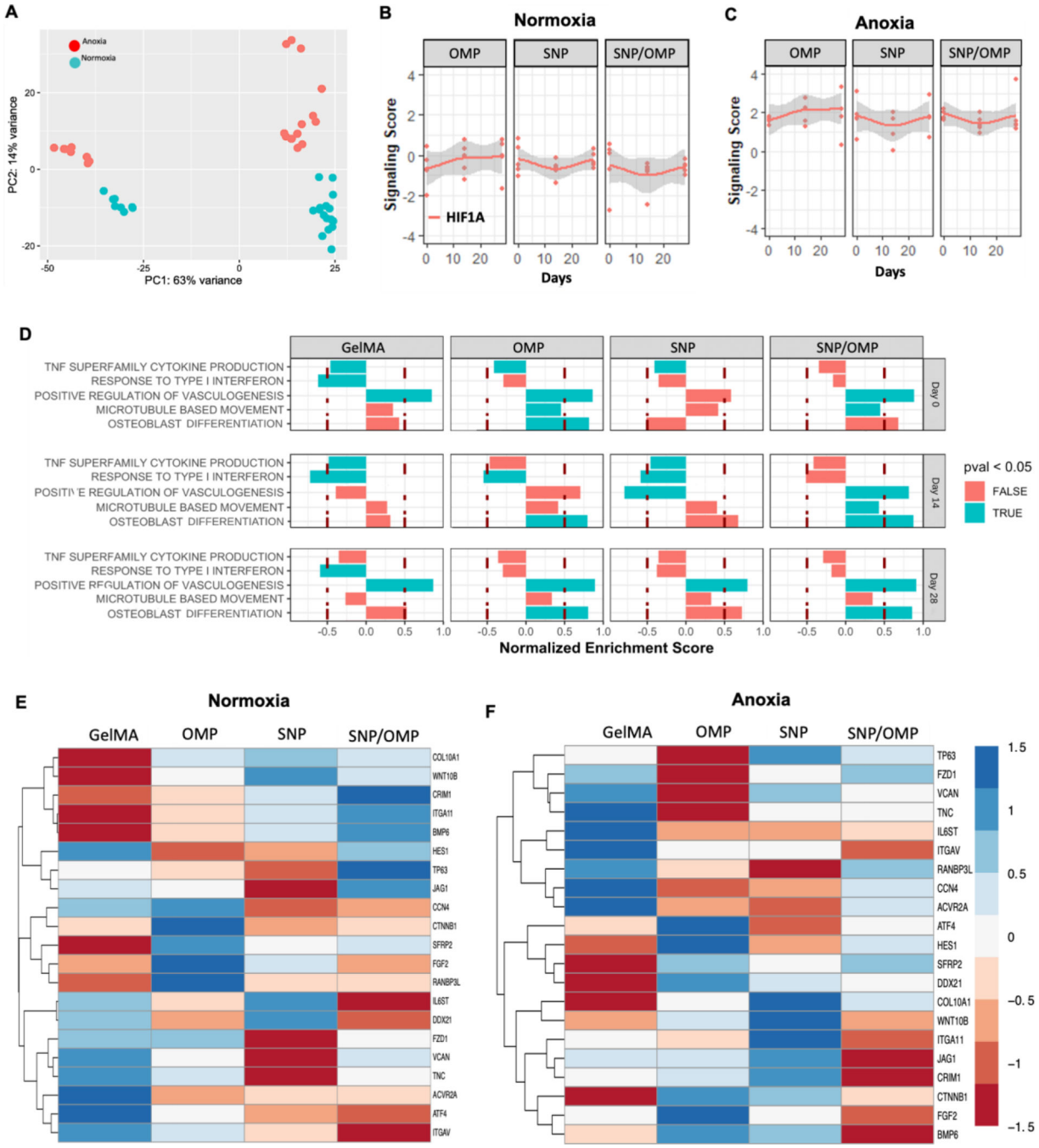

Figure 4: Bulk mRNA analysis of nanocomposite hydrogels containing OMP at different concentrations without and with SNP cultured under either normoxia or anoxia.

(**A**) Global gene expression analyses show an overall enhanced expression under anoxic conditions as compared to normoxia. **(B)** Comparative signaling score analyses of HIF1A under normoxia, and (**C**) anoxia. (**D**) Pathway analysis of the biological processes that were significantly higher in either anoxia (blue) or normoxia (red) after 14 days of culture. Heatmap analysis of osteogenesis-related genes under (**E**) normoxic or zanoxic conditions after 14 days of culture. (n=3).

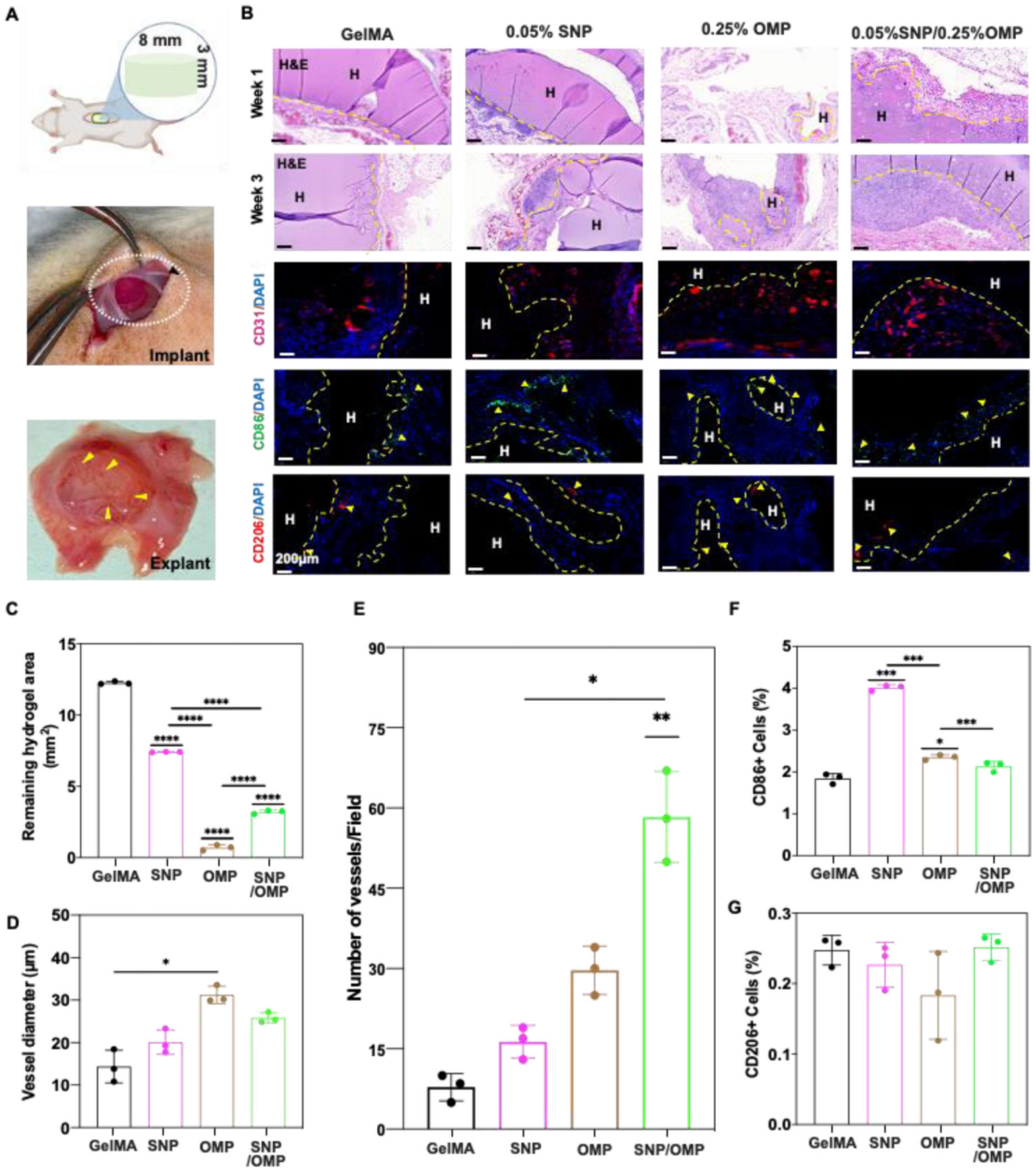

Figure 5: Biodegradation and biocompatibility of SNP/OMP hydrogels after subcutaneous implantation.

(**A**) Schematic representation and photograph depicting the procedure of subcutaneous implantation. (**B**) Microphotographs of histological sections stained with H&E staining 1- and 3 weeks post-implantation or immunohistochemically stained for neovascularization (CD31) or immune response (CD86 and CD206) of different hydrogels without cells 1- or 3-weeks post implantation. Groups: (1) GelMA, (2) SNPs with 0.05% SNP, (3) OMPs with 0.25% OMP, and (4), SNP/OMPs with 0.05% SNP+0.25%OMP. Semi-quantitative image

analyses of (**C**) biodegradation of hydrogels (n=3; ****p<0.0001), (**D**) vessel diameter (n=3; ****p<0.0001), (**E**) number of vessels per field of view (n=3; ***p<0.001, **p<0.01, *p<0.05), (**F**) percentage of CD86+ cells, and (**G**) percentage of CD206+ cells three weeks post-implantation. (n=3; ***p<0.001, *p<0.05).

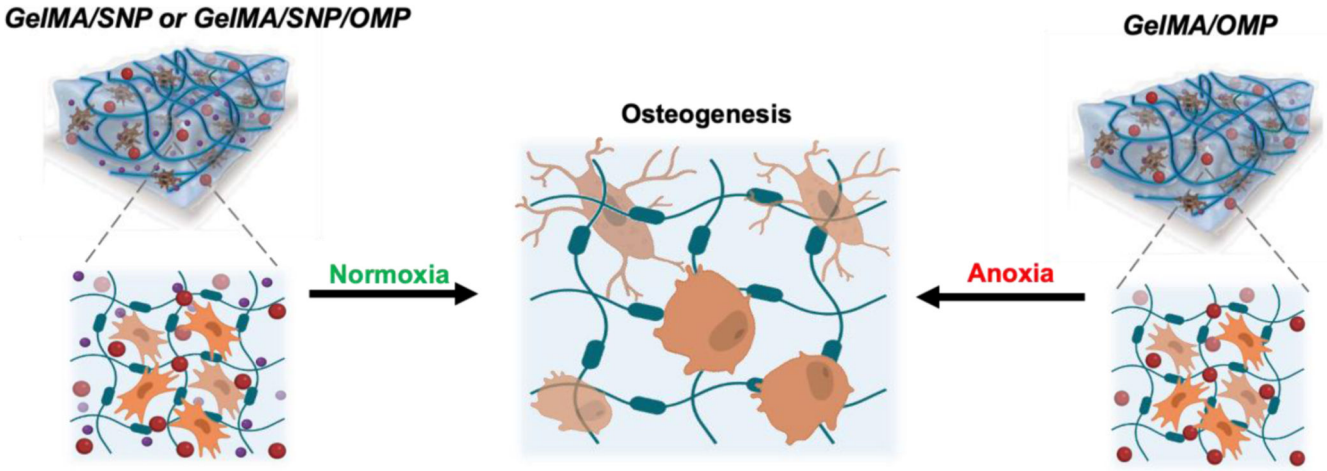

Schematic 1: Depiction of the effect of OMP, SNP, and SNP/OMP on the differentiation fate of hMSCs toward osteogenesis under normoxia and anoxia, respectively.